Switching a polar metal via strain gradients

Asier Zabalo¹ and Massimiliano Stengel^{1, 2}

¹Institut de Ciència de Materials de Barcelona (ICMAB-CSIC), Campus UAB, 08193 Bellaterra, Spain ²ICREA-Institució Catalana de Recerca i Estudis Avanats, 08010 Barcelona, Spain (Dated: November 10, 2021)

Although rare, spontaneous breakdown of inversion symmetry sometimes occurs in a material which is metallic: these are commonly known as polar metals or ferroelectric metals. Their *polarization*, however, cannot be switched via an electric field, which limits the experimental control over band topology. Here we shall investigate, via first-principles theory, flexoelectricity as a possible way around this obstacle with the well known polar metal LiOsO₃. The flexocoupling coefficients are computed for this metal with high accuracy with a completely new approach based on real-space sums of the inter-atomic force constants. A Landau-Ginzburg-Devonshire-type first-principles Hamiltonian is built and a critical bending radius to switch the material is estimated, whose order of magnitude is comparable to that of BaTiO₃.

The so-called polar or ferroelectric metals [1], first proposed by Anderson more than half a century ago in the context of martensitic transformations [2], have been attracting increasing attention recently. The prototypical (and historically the first experimentally known) material realization is lithium osmate, which undergoes a ferroelectric-like transition at 140 K from the centrosymmetric $R\bar{3}c$ to the non-centrosymmetric $R\bar{3}c$ space group [3]. Since its discovery, the list of known polar metals has been steadily growing [4]. Their interest lies on the unusual physics that may emerge from the coexistence of metallicity and polarity, two properties that were initially regarded as contraindicated. For instance, they provide excellent opportunities to study exotic quantum phenomena, like non-centrosymmetric superconductivity [5, 6] or spin-polarized currents [7]. In spite of considerable progress, however, a long-standing issue still remains, and concerns the ability to control polarity via an appropriate external field. Indeed, due to the presence of free carriers in the bulk the most obvious means of switching polarity in ferroelectrics, i.e. an external electric field, is ruled out. Such a control would help shed some light on their fundamental physics, and possibly devise some applications, e.g., in nanoscale electronic and thermoelectric devices [8]. Our goal is to demonstrate that flexoelectricity can solve this issue.

Flexoelectricity describes the coupling between a strain gradient and the macroscopic polarization and, unlike its homogeneous counterpart (piezoelectricity), it does not require any particular space group to be present [9–11]. While flexoelectricity is hardly a new discovery [12], its practical relevance was demonstrated only recently, thus reviving this field from both the experimental [13–15] and theoretical [16] points of view. Of course, the electrical polarization can only be defined in insulating crystals, so the macroscopic flexoelectric coefficient of a polar metal vanishes identically. Hovever, as we shall demonstrate shortly, the coupling between polar lattice modes and a strain gradient does exist even in metals. Since elastic fields, unlike electric fields, are not screened by free

carriers, this constitutes, in principle, a viable means of controlling polarity. Still, whether the relevant couplings are strong enough for such a mechanism to be experimentally accessible, is currently unknown. First-principles calculations could be very helpful in this context, and indeed electronic-structure methods to study flexoelectricity have seen an impressive progress in recent years [16, 17]. However, the calculation of the flexocoupling coefficients remains a subtle task even with insulators and treating metallic crystals falls outside the present capabilities of the density functional theory (DFT) based codes.

Here we overcome such limitations by developing an accurate and general method to calculate flexocoupling coefficients in metals, which is based on real space sums of the inter-atomic force constants (IFC-s). We demonstrate our computational strategy by calculating the flexoccupling coefficients for LiOsO₃ as a test case and we compare them with the ones of BaTiO₃, probably one of the most studied ferroelectric materials. Finally, we use the aforementioned values, in combination with a first-principles based effective Hamiltonian that we have constructed by expanding the energy around the centrosymmetric cubic phase, to estimate the critical bending radius of LiOsO₃. We find the values in line with those calculated for BaTiO₃, a material where flexoelectric switching of the polar domains has been experimentally demonstrated already. Based on these results, mechanical switching of LiOsO₃ mediated by flexoelectricity appears well within experimental reach.

To start with, we shall consider a setup as illustrated in Fig. 1, i.e. of a LiOsO₃ (or n-doped BaTiO₃) sample that is cut along some crystallographic direction \hat{q} and mechanically bent via some external load. Within the interior of the film, the polar order parameter is assumed to be homogeneous, and its amplitude is described by some three-dimensional vector \mathbf{u} with the physical dimension of length. In the following we shall quantify the coercive bending radius, i.e. the radius of curvature that needs to be applied in order to switch the polar order parameter

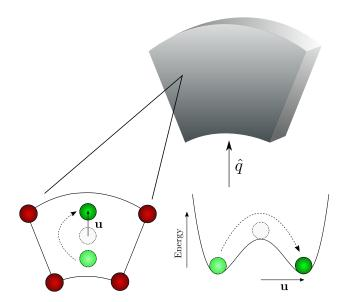


FIG. 1. A bending type strain gradient is applied to a macroscopic crystal along the direction \hat{q} . The external strain gradient couples to the polar modes resulting in a displacement of the atoms and, as a consequence, the structure evolves to another symmetrically equivalent ferroelectric state.

between two neighboring local minima, which are degenerate at mechanical equilibrium. We shall calculate the critical radius via the following formula,

$$R_{\rm crit} = \frac{f_{\rm eff}}{F_{\rm coerc}},$$
 (1)

where $f_{\rm eff}$ is the effective flexocoupling coefficient associated with the flexural deformation, and $F_{\rm coerc}$ is the minimal generalized force that is required for the mode ${\bf u}$ to cross the energy barrier between two minima. Thus, the problem can be divided into two separate tasks: (i) determining the coupling between a flexural deformation and the polar mode, described by $f_{\rm eff}$, as a function of the crystallographic orientation, and (ii) identifying the most likely switching paths and the corresponding energetics.

From now on, we shall assume a Landau-like expansion of the energy around the high-symmetry cubic structure as a function of the relevant parameters, following the established common practice in theoretical studies of perovskite ferroelectrics. In this context, task (ii) entails no conceptual difficulties, as it consists in mapping the potential energy surface of the crystal as a function of the relevant lattice degrees of freedom – such a procedure has been successfully carried out for a wide range of materials already. The main technical obstacle resides in (i), since no established methods exist for the calculation of $f_{\rm eff}$ in metals. Given the novelty, we shall focus on this point in the following.

In full generality, the flexocoupling tensor in a "soft-

mode" material can be defined as follows [18],

$$f_{\alpha\beta,\gamma\lambda}^{\rm I} = -\frac{M}{2} \langle P_{\alpha} | \frac{\partial^2 D(\mathbf{q})}{\partial q_{\gamma} \partial q_{\lambda}} \Big|_{\mathbf{q}=0} |A_{\beta}\rangle$$
 (2)

where $D(\mathbf{q})$ is the dynamical matrix of the crystal at a certain wavevector \mathbf{q} , and the bra and kets represent the TO₁ and acoustic eigenvectors at the Γ ($\mathbf{q} = 0$) point of the Brillouin zone. This tensor describes the force on u_{α} that is produced by a macroscopic strain gradient $\eta_{\beta,\gamma\lambda}$, the latter expressed in "type-I" form (hence the superscript "I"), i.e., as the second gradient of the displacement field. For our present scopes, it is more convenient to work in type-II form, which can be recovered via the following transformation,

$$f_{\alpha\lambda,\beta\gamma}^{\mathrm{II}} = f_{\alpha\beta,\gamma\lambda}^{\mathrm{I}} + f_{\alpha\gamma,\lambda\beta}^{\mathrm{I}} - f_{\alpha\lambda,\beta\gamma}^{\mathrm{I}}.$$
 (3)

The main technical challenge from a computational point of view consists in taking the second gradient with respect to \mathbf{q} of the dynamical matrix, $D(\mathbf{q})$. In insulators, this task is already delicate at the formal level, since $D(\mathbf{q})$ has a *nonanalytic* behavior in vicinity of Γ ; this requires a careful treatment of the macroscopic electric fields before performing the perturbative long-wave expansion. In metals at finite temperature things appear simpler conceptually, since the adiabatic dynamical matrix $D(\mathbf{q})$ is an analytic function of the wavevector **q** over the whole Brillouin zone. This means that the second q-gradient appearing in Eq. (2) is always well defined without taking any further precaution. However, this methodology has not been generalized to metals yet. To circumvent this obstacle, we define the long-wave expansion of the dynamical matrix as the real-space moments of the interatomic force constants, following the method described in [11, 18]. In particular, the IFC's are first defined as the second derivative of the total energy with respect to atomic displacements,

$$\Phi^{l}_{\kappa\alpha,\kappa'\beta} = \frac{\partial^{2} E}{\partial u^{0}_{\kappa\alpha} \partial u^{l}_{\kappa'\beta}}.$$
 (4)

Then, we write

$$\left. \frac{\partial^2 D_{\kappa\alpha,\kappa'\beta}^{(\mathbf{q})}}{\partial q_{\gamma} \partial q_{\lambda}} \right|_{\mathbf{q}=0} = \sum_{l} \frac{\Phi_{\kappa\alpha,\kappa'\beta}^{l}}{\sqrt{m_{\kappa} m_{\kappa'}}} (\mathbf{d}_{\kappa\kappa'}^{l})_{\gamma} (\mathbf{d}_{\kappa\kappa'}^{l})_{\lambda}, \quad (5)$$

where m_{κ} is the mass of atom κ , $\mathbf{d}_{\kappa\kappa'}^{l} = \mathbf{R}^{l} + \boldsymbol{\tau}_{\kappa'} - \boldsymbol{\tau}_{\kappa}$, \mathbf{R}^{l} is the Bravais lattice vector indicating the location of the l-th cell and $\boldsymbol{\tau}_{\kappa}$ is the position of atom κ within the unit cell l=0. The short-range nature of the interatomic forces guarantees that the lattice sums of Eq. (5) will eventually converge to the correct physical value when a dense enough \mathbf{q} -point mesh is used to calculate the real-space force constants of Eq. (4). Interestingly, the coupling between two acoustic modes is directly related

TABLE I. Independent components of the elastic (in GPa) and flexocoupling (in eV) tensor with a $16 \times 16 \times 1$ mesh of **q** points for the IFC-s. The n-type flexocoupling coefficients of BaTiO₃ are shown here.

					$f_{11}^{ m II}$		
LiOsO ₃	Long-wave	364.7	129.5	44.3	-13.8	49.3	3.3
	DFPT	365.6	129.5	44.1		_	
BaTiO ₃	Long-wave	346.1	121.7	134.5	-53.5	3.4	-39.5
	DFPT	353.3	121.7	137.7	_	_	_

(in a crystal that is free of stresses) to the elastic tensor components via [19]

$$\frac{C_{\alpha\gamma,\beta\lambda} + C_{\alpha\lambda,\beta\gamma}}{2} = -\frac{M}{2\Omega} \left\langle A_{\alpha} \right| \frac{\partial^{2} D(\mathbf{q})}{\partial q_{\gamma} \partial q_{\lambda}} \bigg|_{\mathbf{q}=0} \left| A_{\beta} \right\rangle. \quad (6)$$

This is a useful consistency check: one can then compare the results with a more conventional calculation of the elastic tensor [20] to gauge the reliability of the flexocoupling coefficients as determined via Eq. (2). Note that the elastic tensor components are themselves a crucial ingredient for calculating the effective flexocoupling of Eq. (1) starting from the flexocoupling tensor \mathbf{f}^{II} ; therefore, it is important to ensure that the two physical quantities are calculated with consistent accuracy.

Our first principles calculations are performed with the open-source ABINIT [21, 22] package. (Details of the computational parameters are provided in the Supplementary Material.) Numerical results for both BaTiO₃ and LiOsO₃ are shown in Table I. Clearly, the largest flexocouplings are f_{12} in LiOsO₃ and f_{11} for BaTiO₃. (The latter material behaves very similarly to SrTiO₃ [18], which is natural to expect given the affinities in the electronic and atomic structure.) Their absolute values are similar overall, which provides a first indication that the flexocoupling is comparably strong in these two materials. Note that the discrepancy in the elastic constants calculated via the two different methods is less than a 1 % for the three independent components of LiOsO₃, which confirms the excellent quality of the calculations. We also show in Fig. S3 (and Table S4) the convergence of the numerical results for both the elastic and flexocoupling constants as a function of the **q**-point mesh, further corroborating this point.

To make further progress, we use the value of Table I to compute the effective flexocoupling coefficients for three representative orientations of the sample ([100], [110] and [111]), either in the beam-bending or the plate-bending limit. (We focus on the beam-bending limit following the definitions of Ref. [23]; explicit formulas are reported in the Supplementary Material.) The results, shown in Table II, indicate that [100] is by far the bending direction that produces the largest flexocoupling in LiOsO₃. The situation in BaTiO₃ seems to be more balanced overall,

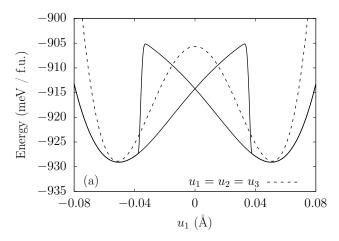
TABLE II. Effective flexocoupling coefficients (absolute values) for 100, 110 and 111 oriented samples (in eV units) for the beam-bending limit.

	$f_{ m eff}^{100}$	$f_{ m eff}^{110}$	$f_{ m eff}^{111}$
${\rm LiOsO_3}$	40.1	5.3	2.5
$BaTiO_3$	16.2	24.7	23.3

with a slight preference for [110] and [111] directions over [100]. Note, however, that for each surface orientation $\hat{\mathbf{q}}$, the effective flexocoupling describes the flexo-induced force acting on the polar mode along $\hat{\mathbf{q}}$. Depending on the switching path, such force might not be parallel to the direction along which the polar mode evolves during switching, $\hat{\mathbf{s}}$; in such cases the effective flexocoupling needs to be scaled by the projection $\hat{\mathbf{q}} \cdot \hat{\mathbf{s}}$. Since the relevant paths in BaTiO₃ (see next paragraph) involve [100]-oriented switching, such geometrical factor reduces the [110] and [111] coefficients by $\sqrt{2}$ and $\sqrt{3}$ respectively, bringing all three values of $f_{\rm eff}$ to a similar magnitude.

Having calculated the values of f_{eff} , we now need the information about the switching path to obtain $R_{\rm crit}$ according to Eq. (1). To this end, we construct a Landau-Ginzburg-Devonshire-type first-principles Hamiltonian by expanding the energy around the reference cubic phase, of $Pm\bar{3}m$ symmetry. The Hamiltonian includes the most important degrees of freedom of the structure: the strain s_{ij} , the tilts of the oxygen octahedra q_i , where q_i represents the displacements of the oxygen atoms perpendicular to the rotation axis and the polar modes u_i . (Details on the model can be found in the Supplementary Material.) First, we validate our effective Hamiltonian H_{eff} by calculating the energetics of the relevant phases (Table S2) and their variation as a function of external pressure (Fig. S1); in both cases we obtain excellent agreement to the first-principles results. Next, we proceed to calculating the most favorable switching paths by constraining one component of the polar vector [24, 25] and numerically minimizing (simulated annealing) the energy functional with respect to the other parameters.

The resulting double-well potential curves of LiOsO₃ and BaTiO₃ are shown in Fig. 2. Before commenting on the results, it is useful to recall the structural properties of each of the two materials. The structural ground state of LiOsO₃ has R3c symmetry, containing both polar distortions and antiphase octahedral tilts ($a^-a^-a^-$ in Glazer notation) oriented along the [111] pseudocubic direction. Since the energy scale associated to the AFD distortions is an order of magnitude larger than that associated to $\bf u$, they are unlikely to be affected by a weak elastic field; in practice, $\bf u$ can only switch between the [111] and [$\bar{1}\bar{1}\bar{1}$] states. Regarding the actual switching path, two scenarios are in principle possible. If



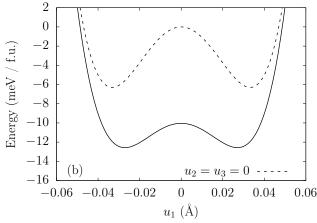


FIG. 2. Potential energy landscape for LiOsO₃ (a) and BaTiO₃ (b) from our first principles effective Hamiltonians, obtained by minimizing the energy at fixed u_1 . For LiOsO₃, a double-well like curve is obtained when $u_1 = u_2 = u_3$ is enforced (dashed line) and a butterfly-like diagram is obtained when all the parameters are allowed to evolve freely (solid line). For BaTiO₃, the dashed line represents the study under the $u_2 = u_3 = 0$ constraint, and the solid line the case with no constraints.

the non-polar $R\bar{3}c$ structure were stable under the constraint $u_1 = 0$, the polar modes would be forced to evolve along the same pseudocubic [111] direction even under the action of a [100]-oriented external force. However, previous first-principles calculations have shown [26] that the $R\bar{3}c$ phase has more than one imaginary mode at Γ , which means that $R\bar{3}c$ is unlikely to be the saddle point. This suspicion is nicely confirmed by the results of our effective Hamiltonian: indeed, the "butterfly diagram" of Fig. 2 clearly reflects the presence of a switchable in-plane polarization at $u_1 = 0$; the resulting coercive field is $F_{\text{coerc}}=0.34 \text{ eV/Å}$. To quantify how much the system gains by circumnavigating the energy barrier, we attempted the same computational experiment while imposing $u_1 = u_2 = u_3$ along the path; as expected, we obtain a substantially larger critical field of $F_{\text{coerc}}=0.69$

eV/Å, assuming that the field is still applied along [100].

For BaTiO₃ the polarization cannot be constrained by the tilts, since the latter are absent in this material. At low-temperature $BaTiO_3$ has R3m symmetry, and we find that the lowest switching barrier occurs when the polarization continuously rotates from [111] to $[\bar{1}11]$ by passing through an orthorhombic [110] saddle point. (The path is roughly oriented along [100]). We find a critical coercive field of F_{coerc} =0.14 eV/Å for such a switching path. For comparison to room-temperature experiments, where BaTiO₃ adopts a tetragonal structure, we also calculate the hypothetical barrier that one would obtain by constraining $\mathbf{P} \parallel [100]$ (i.e. by setting the in-plane components of **P** to zero). We find $F_{\text{coerc}}=0.29 \text{ eV/Å}$. This is a substantially larger value than the aforementioned threshold for polarization rotation, in line with literature results.

We are now ready to answer the main physical question we asked to ourselves at the beginning: how much do we need to bend a LiOsO₃ sample to reverse its polar lattice distortion? By means of Eq. (1) we can compute the critical bending radius for both materials. The obtained values are $R_{\rm crit} \sim 118$ Å for LiOsO₃ and $R_{\rm crit} \sim 125$ Å for rhombohedral BaTiO₃ and $R_{\rm crit} \sim 60$ Å for tetragonal BaTiO₃. Remarkably, the calculated critical bending radius of LiOsO₃ is twice as large as that of tetragonal BaTiO₃, essentially matching the calculated value of rhombohedral BaTiO₃. Since mechanical switching of polar domains in tetragonal barium titanate has already been experimentally achieved [27] via strain gradients, our results indicate that this is very likely to be feasible in LiOsO₃ as well.

Our results for BaTiO₃ are in good agreement with the ones reported in Ref. [28] where a critical bending radius of 110 Å was estimated. This is substantially smaller than the available experimental estimates (a value of $R_{\rm crit} \sim 300 \text{ Å was observed in BaTiO}_3$ [27]). This is expected: theoretical estimations of coercive fields in ferroelectrics that are based on the homogeneous Landau potential are typically overestimated by one or two orders of magnitude [29]. Consideration of more realistic mechanisms (e.g., domain wall nucleation and motion) would drastically complicate our study, and bring us far from our main scopes. We stress in any case, that our underestimation of the critical bending radii compared to experiments should be ascribed to an overestimation of F_{crit} , while we regard our calculation of the flexocouplings as accurate. (The contribution of the oxygen octahedral tilt gradients to the flexocoupling in lithium osmate was neglected in this work. While certainly present, we consider it unlikely to qualitatively affect our conclusions; it will be an interesting topic for follow-up studies.)

We expect our results to significantly broaden the scopes of both flexoelectricity and the ongoing search for new functionalities based on polar metals. In this sense, we believe that our work may open several unexplored

research directions. First and foremost, we regard an experimental verification of our predictions as the most pressing priority. Second, it will be interesting to estimate the magnitude of the flexocouplings in a broader range of polar metals, and identify candidates where the effect is especially strong. Finally, from the point of view of the theory, developing the methodological tools to assess the impact of tilt gradients on the calculated coefficients is another topic that we regard as promising for future studies.

We acknowledge the support of Ministerio de Economia, Industria y Competitividad (MINECO-Spain) through Grants No. MAT2016-77100-C2-2-P and No. SEV-2015-0496, and of Generalitat de Catalunya (Grant No. 2017 SGR1506). This project has received funding from the European Research Council (ERC) under the European Union's Horizon 2020 research and innovation program (Grant Agreement No. 724529). Part of the calculations were performed at the Supercomputing Center of Galicia (CESGA).

- T. Kim, D. Puggioni, Y. Yuan, L. Xie, H. Zhou, N. Campbell, P. Ryan, Y. Choi, J.-W. Kim, J. Patzner, et al., Nature 533, 68 (2016).
- [2] P. W. Anderson and E. Blount, Physical Review Letters 14, 217 (1965).
- [3] Y. Shi, Y. Guo, X. Wang, A. J. Princep, D. Khalyavin, P. Manuel, Y. Michiue, A. Sato, K. Tsuda, S. Yu, et al., Nature materials 12, 1024 (2013).
- [4] N. A. Benedek and T. Birol, Journal of Materials Chemistry C 4, 4000 (2016).
- [5] E. Bauer and M. Sigrist, Non-centrosymmetric superconductors: introduction and overview, Vol. 847 (Springer Science & Business Media, 2012).
- [6] S. Yip, Annu. Rev. Condens. Matter Phys. 5, 15 (2014).
- [7] C.-K. Lu and S. Yip, Physical Review B 82, 104501 (2010).
- [8] C. Ma and K. Jin, SCIENCE CHINA Physics, Mechanics & Astronomy 61, 97011 (2018).

- [9] M. Stengel and D. Vanderbilt, (2016).
- [10] P. Yudin and A. Tagantsev, Nanotechnology 24, 432001 (2013).
- [11] M. Stengel, Physical Review B 88, 174106 (2013).
- [12] S. M. Kogan, Soviet Physics-Solid State 5, 2069 (1964).
- [13] F. Vasquez-Sancho, A. Abdollahi, D. Damjanovic, and G. Catalan, Advanced materials 30, 1705316 (2018).
- [14] J. Narvaez, F. Vasquez-Sancho, and G. Catalan, Nature 538, 219 (2016).
- [15] H. Lu, C.-W. Bark, D. E. De Los Ojos, J. Alcala, C.-B. Eom, G. Catalan, and A. Gruverman, Science 336, 59 (2012).
- [16] M. Royo and M. Stengel, Physical Review X 9, 021050 (2019).
- [17] M. Stengel and D. Vanderbilt, in Flexoelectricity in Solids: From Theory to Applications (World Scientific, 2017) pp. 31–110.
- [18] M. Stengel, Physical Review B 93, 245107 (2016).
- [19] M. Born and K. Huang, Dynamical theory of crystal lattices (Clarendon press, 1954).
- [20] X. Wu, D. Vanderbilt, and D. Hamann, Physical Review B 72, 035105 (2005).
- [21] X. Gonze, B. Amadon, P.-M. Anglade, J.-M. Beuken, F. Bottin, P. Boulanger, F. Bruneval, D. Caliste, R. Caracas, M. Côté, et al., Computer Physics Communications 180, 2582 (2009).
- [22] X. Gonze, B. Amadon, G. Antonius, F. Arnardi, L. Baguet, J.-M. Beuken, J. Bieder, F. Bottin, J. Bouchet, E. Bousquet, et al., Computer Physics Communications 248, 107042 (2020).
- [23] J. Narvaez, S. Saremi, J. Hong, M. Stengel, and G. Catalan, Physical review letters 115, 037601 (2015).
- [24] O. Diéguez and D. Vanderbilt, Physical review letters 96, 056401 (2006).
- [25] M. Stengel, N. A. Spaldin, and D. Vanderbilt, Nature Physics 5, 304 (2009).
- [26] H. Sim and B. G. Kim, Physical Review B 89, 201107 (2014).
- [27] J. Očenášek, H. Lu, C. Bark, C.-B. Eom, J. Alcalá, G. Catalan, and A. Gruverman, Physical Review B 92, 035417 (2015).
- [28] G. Li, X. Huang, J. Hu, and W. Zhang, Physical Review B 95, 144111 (2017).
- [29] V. Shelke, D. Mazumdar, G. Srinivasan, A. Kumar, S. Jesse, S. Kalinin, A. Baddorf, and A. Gupta, Advanced Materials 23, 669 (2011).

Supplementary notes for "Switching a polar metal via strain gradients"

Asier Zabalo¹ and Massimiliano Stengel^{1, 2}

¹Institut de Ciència de Materials de Barcelona (ICMAB-CSIC), Campus UAB, 08193 Bellaterra, Spain ²ICREA-Institució Catalana de Recerca i Estudis Avanats, 08010 Barcelona, Spain

I. COMPUTATIONAL DETAILS

Calculations on LiOsO₃ are carried out with pseudopotentials under the generalized gradient approximation (GGA) with Perdew-Burke-Ernzerhof (PBE) exchange-correlation functionals [1]. A dense $16 \times 16 \times 16$ k-point mesh is used to sample the Brillouin zone with a plane-wave cutoff of 60 Ha. A Gaussian smearing of 0.01 Ha is applied and effects of spin-orbit coupling are neglected [2]. The dynamical properties, i.e., phonon frequencies and eigenmodes, are calculated using DFPT as implemented in ABINIT. The independent components of both the elastic and the flexocoupling tensor are computed with Eq. (2) and Eq. (6) of the main text and convergence is tested with respect to the two-dimensional grid of $\bf q$ points. For cubic systems a two dimensional grid is enough to calculate the three independent components of the mentioned tensors, commonly denoted as longitudinal (C_{11}, f_{11}) , transverse (C_{12}, f_{12}) and shear (C_{44}, f_{44}) . For a $16 \times 16 \times 1$ mesh of $\bf q$ points convergence was clearly reached for the elastic constants, and as a consequence, for the flexocoupling tensor. (Remember that both calculations are carried out using exactly the same method, so a similar convergence rate and errors are expected.) Calculations for BaTiO₃ are performed by using LDA and a $12 \times 12 \times 12$ k-point mesh, and the flexocoupling coefficients are extracted via the method described in Ref. [3]. For a meaningful comparison with metallic LiOsO₃ we use the conduction band bottom as energy reference, which yields the n-type flexocoupling coefficients as defined in Ref. [3]. (Note that the f_{44} component is independent of such a choice.)

II. FIRST-PRINCIPLES EFFECTIVE HAMILTONIAN OF LIOSO3

Expression and parameters The explicit expression for the first-principles Hamiltonian of LiOsO₃, which gives the energy of a 10-atom cell, is the following:

$$\begin{split} H &= \frac{\Omega}{2} C_{11}(s_1^2 + s_2^2 + s_3^2) + \Omega C_{12}(s_1 s_2 + s_1 s_3 + s_2 s_3) + \frac{\Omega}{2} C_{44}(s_4^2 + s_5^2 + s_6^2) \\ &+ \beta_1(q_1^2 + q_2^2 + q_3^2) + \beta_2(q_1^4 + q_2^4 + q_3^4) + \beta_3(q_2^2 q_3^2 + q_1^2 q_3^2 + q_1^2 q_2^2) \\ &+ \zeta_1(u_1^2 + u_2^2 + u_3^2) + \zeta_2(u_1^4 + u_2^4 + u_3^4) + \zeta_3(u_2^2 u_3^2 + u_1^2 u_3^2 + u_1^2 u_2^2) \\ &+ \zeta_4(u_1^6 + u_2^6 + u_3^6) + \zeta_5[u_1^4(u_2^2 + u_3^2) + u_2^4(u_1^2 + u_3^2) + u_3^4(u_1^2 + u_2^2)] \\ &+ \zeta_6(u_1^8 + u_2^8 + u_3^8) \\ &+ \lambda_1(s_1q_1^2 + s_2q_2^2 + s_3q_3^2) + \lambda_2[s_1(q_2^2 + q_3^2) + s_2(q_1^2 + q_3^2) + s_3(q_1^2 + q_2^2)] \\ &+ \lambda_3(s_4q_2q_3 + s_5q_1q_3 + s_6q_1q_2) + \lambda_4(s_1q_1^4 + s_2q_2^4 + s_3q_3^4) \\ &+ \lambda_5(s_4q_2^2q_3^2 + s_5q_1^2q_3^2 + s_6q_1^2q_2^2) \\ &+ \rho_1(s_1u_1^2 + s_2u_2^2 + s_3u_3^2) + \rho_2[s_1(u_2^2 + u_3^2) + s_2(u_1^2 + u_3^2) + s_3(u_1^2 + u_2^2)] \\ &+ \rho_3(s_4u_2u_3 + s_5u_1u_3 + s_6u_1u_2) + \rho_4(s_1u_1^4 + s_2u_2^4 + s_3u_3^4) \\ &+ \rho_5(s_4u_2^2u_3^2 + s_5u_1^2u_3^2 + s_6u_1^2u_2^2) \\ &+ \rho_6[s_1(u_2^4 + u_3^4) + s_2(u_1^4 + u_3^4) + s_3(u_1^4 + u_2^4)] \\ &+ \gamma_1(u_1^2q_1^2 + u_2^2q_2^2 + u_3^2q_3^2) + \gamma_2(u_1^2q_1^4 + u_2^2q_2^4 + u_3^2q_3^4). \end{split}$$

where the strain is given in the matrix Voigt notation. The calculated model parameters are given in Table S1.

TABLE S1. Calculated model parameters for the first-principles Hamiltonian of $LiOsO_3$.

Parameter	Value	Units	Parameter	Value	Units
Ω	112.94	$\mathring{\mathrm{A}}^3$	λ_1	38.2516	$eV/\text{Å}^2$
C_{11}	365.58	GPa	λ_2	19.0951	$\mathrm{eV/\mathring{A}}^2$
C_{12}	129.48	GPa	λ_3	-12.3815	$\mathrm{eV/\mathring{A}}^2$
C_{44}	44.09	GPa	λ_4	-32.8244	$\mathrm{eV/\AA}^4$
eta_1	-4.31776	$\mathrm{eV/\mathring{A}}^2$	λ_5	16.3332	$\mathrm{eV/\AA}^4$
eta_2	8.03626	$\mathrm{eV/\mathring{A}}^4$	$ ho_1$	81.4362	$\mathrm{eV/\mathring{A}}^2$
eta_3	5.97264	$\mathrm{eV/\mathring{A}}^4$	$ ho_2$	-136.627	$\mathrm{eV/\mathring{A}}^2$
ζ_1	-35.4382	$\mathrm{eV/\mathring{A}}^2$	$ ho_3$	-110.971	$\mathrm{eV/\mathring{A}}^2$
ζ_2	868.601	$\mathrm{eV/\mathring{A}}^4$	$ ho_4$	-308.951	$\mathrm{eV/\AA}^4$
ζ_3	2205.6	$\mathrm{eV/\mathring{A}}^4$	$ ho_5$	-14380.5	$\mathrm{eV/\AA}^4$
ζ_4	-6978.34	$\mathrm{eV/\mathring{A}}^6$	$ ho_6$	-11808.3	$\mathrm{eV/\AA}^4$
ζ_5	59153.0	$\mathrm{eV/\mathring{A}}^6$	γ_1	348.113	${ m eV/\AA}^4$
ζ_6	20643.6	$\mathrm{eV/\mathring{A}^8}$	γ_2	-990.2	$\mathrm{eV/\mathring{A}}^{6}$

Validation of the model As a first test of the model we compute the energy of the most relevant phases that can be obtained by combining antiferrodistortive and polar instabilities, compared with the reference $Pm\bar{3}m$ structure. This is, of course, the structural ground state of R3c symmetry, containing both polar distortions and antiphase octahedral tilts ($a^-a^-a^-$ in Glazer notation) oriented along the [111] pseudocubic direction. Other important phases are the centrosymmetric $R\bar{3}c$ and the polar R3m, where either the polar or the antiferrodistortive modes are suppressed. As we can see from the calculated values (Table S2), the model accurately reproduces the first-principles results obtained by fully relaxing the crystal cell within the given symmetry. In particular, this first-principles Hamiltonian almost perfectly describes the energy difference between the lowest-energy $R\bar{3}c$ and the R3c phases, which are the most relevant for ferroelectric switching: -22 meV/f.u. with DFT and -23 meV/f.u. with our Hamiltonian, were f.u. stands for perovskite formula unit. As a further test, we study the phase diagram of LiOsO₃ as a function of cell volume. The dots shown in Fig. S1 were obtained via explicit DFT calculations by fully relaxing the ionic positions for each fixed cell volume. These results are in excellent agreement with experimental values [4] and previous first-principles studies [5]. Solid lines represent the energies obtained with our model, again showing excellent agreement with the first-principles values.

TABLE S2. Volume and energy comparison between first-principles calculations and our model. Energies are in meV /.f.u. units.

	DFT		Effective Hamiltonian	
	ΔE	$\Delta V(\%)$	ΔE	$\Delta V(\%)$
R3m	-149	1.1	-157	1.3
$R\bar{3}c$	-908	-11.4	-906	-11.5
R3c	-930	-12.0	-929	-11.9

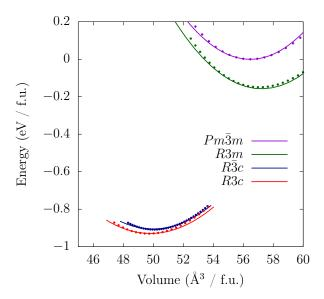


FIG. S1. Energy per formula unit as a function of the volume of the perovskite formula unit of $Pm\bar{3}m$, R3m, $R\bar{3}c$, and R3c phases. Solid lines are obtained from our effective Hamiltonian.

III. FIRST-PRINCIPLES EFFECTIVE HAMILTONIAN OF Batio₃

Expression and parameters The explicit expression for the first-principles Hamiltonian of BaTiO₃, which gives the energy of a 5-atom cell, is the following:

$$H = \frac{\Omega}{2}C_{11}(s_1^2 + s_2^2 + s_3^2) + \Omega C_{12}(s_1s_2 + s_1s_3 + s_2s_3) + \frac{\Omega}{2}C_{44}(s_4^2 + s_5^2 + s_6^2)$$

$$+ \zeta_1(u_1^2 + u_2^2 + u_3^2) + \zeta_2(u_1^4 + u_2^4 + u_3^4) + \zeta_3(u_2^2u_3^2 + u_1^2u_3^2 + u_1^2u_2^2)$$

$$+ \rho_1(s_1u_1^2 + s_2u_2^2 + s_3u_3^2) + \rho_2[s_1(u_2^2 + u_3^2) + s_2(u_1^2 + u_3^2) + s_3(u_1^2 + u_2^2)]$$

$$+ \rho_3(s_4u_2u_3 + s_5u_1u_3 + s_6u_1u_2) + \rho_4(s_1u_1^4 + s_2u_2^4 + s_3u_3^4)$$

$$+ \rho_5(s_4u_2^2u_3^2 + s_5u_1^2u_3^2 + s_6u_1^2u_2^2)$$

$$+ \rho_6[s_1(u_2^4 + u_3^4) + s_2(u_1^4 + u_3^4) + s_3(u_1^4 + u_2^4)]$$

$$(2)$$

The calculated model parameters are given in Table S3.

Parameter	Value	Units	Parameter	Value	Units
Ω	60.745	Å ³	$ ho_1$	-911.228	$eV/\text{Å}^2$
C_{11}	353.30	GPa	$ ho_2$	-97.0643	$\mathrm{eV/\mathring{A}}^2$
C_{12}	121.75	GPa	$ ho_3$	-99.2179	$\mathrm{eV/\mathring{A}}^2$
C_{44}	137.72	GPa	$ ho_4$	-29262.0	$\mathrm{eV/\AA}^4$
ζ_1	-11.5402	$eV/\text{Å}^2$	$ ho_5$	31131.0	$\mathrm{eV/\AA}^4$
ζ_2	7294.25	$\mathrm{eV/\mathring{A}}^4$	$ ho_6$	9691.01	$\mathrm{eV/\AA}^4$
ζ_3	3441.25	$\mathrm{eV/\mathring{A}}^4$	_	_	_

TABLE S3. Calculated model parameters for the first-principles Hamiltonian of BaTiO₃.

Validation of the model As with lithium osmate, we first compute the energy of the relevant phases. Since there are no tilts, this reduces to calculating the energy of the ground state R3m phase. Fig. S2 shows the phase diagram of the cubic and R3m phases as a function of cell volume, showing an excellent agreement with the first principles calculations.

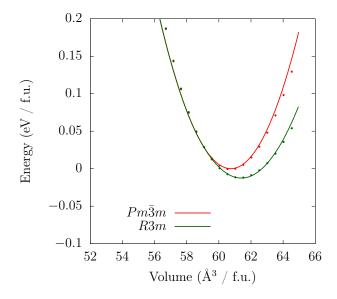


FIG. S2. Energy per formula unit as a function of the volume of the perovskite formula unit of $Pm\bar{3}m$ and R3m phases of BaTiO₃. Solid lines are obtained from our effective Hamiltonian.

IV. FLEXOCOUPLING COEFFICIENTS

Convergence of flexocoupling coefficients The convergence of the flexocoupling coefficients (in the type-II representation) of $LiOsO_3$ with respect to the **q** point mesh, for a fixed **k** point mesh, is analyzed. Numerical values are shown in Table S4 and graphical results are given in Fig. S3.

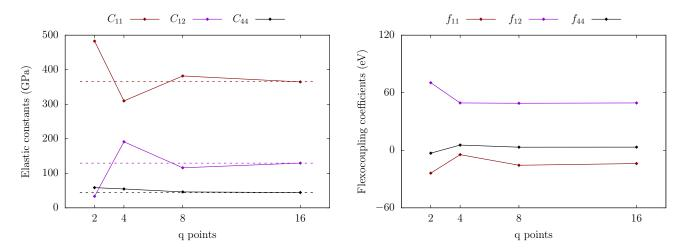


FIG. S3. Convergence of the elastic tensor and the flexocoupling tensor with respect to the two-dimensional grid of q points $(q \times q \times 1)$. The dashed lines represent the reference values of the elastic constants, computed with DFPT. Only the three independent components are shown.

		<u> </u>		<u> </u>
grid of q points	$2 \times 2 \times 1$	$4 \times 4 \times 1$	$8 \times 8 \times 1$	$16 \times 16 \times 1$
C_{11}	482.93	309.66	381.90	364.72
C_{12}	33.45	191.35	115.92	129.54
C_{44}	58.46	54.63	46.13	44.30
$f_{11}^{ m II}$	-23.84	-4.53	-15.62	-13.82
$f_{12}^{ m II}$	70.42	49.34	49.02	49.35
$f_{44}^{ m II}$	-3.43	5.43	3.24	3.27

TABLE S4. Independent components of the elastic tensor (in GPa) and the flexocoupling tensor (in eV).

Effective flexocoupling coefficients In order to have a self contained manuscript, here we give the expressions of the effective flexocoupling coefficients for the [100], [110] and [111] orientations for the beam-bending limit following the definitions of Ref. [6].

$$f_{\text{eff}}^{100} = \frac{-C_{12}}{C_{11} + C_{12}} f_{11}^{\text{II}} + \frac{C_{11}}{C_{11} + C_{12}} f_{12}^{\text{II}},$$

$$f_{\text{eff}}^{110} = A f_{11}^{\text{II}} + B f_{12}^{\text{II}} - 2(1 - A) f_{44}^{\text{II}},$$

$$f_{\text{eff}}^{111} = \frac{C_{44}}{C_{11} + 2C_{12} + C_{44}} (f_{11}^{\text{II}} + 2f_{12}^{\text{II}}) - \frac{C_{11} + 2C_{12}}{C_{11} + 2C_{12} + C_{44}} f_{44}^{\text{II}},$$
(3)

where

$$A = \frac{2C_{11}C_{44}}{(C_{11} - C_{12})(C_{11} + 2C_{12}) + 2C_{11}C_{44}},$$

$$B = \frac{2(C_{11} - 2C_{12})C_{44}}{(C_{11} - C_{12})(C_{11} + 2C_{12}) + 2C_{11}C_{44}}.$$
(4)

- [1] J. P. Perdew, K. Burke, and M. Ernzerhof, Physical review letters 77, 3865 (1996).
- [2] N. A. Benedek and T. Birol, Journal of Materials Chemistry C 4, 4000 (2016).
- [3] M. Stengel, Physical Review B **93**, 245107 (2016).
- [4] Y. Shi, Y. Guo, X. Wang, A. J. Princep, D. Khalyavin, P. Manuel, Y. Michiue, A. Sato, K. Tsuda, S. Yu, et al., Nature materials 12, 1024 (2013).
- [5] H. Sim and B. G. Kim, Physical Review B 89, 201107 (2014).
- [6] J. Narvaez, S. Saremi, J. Hong, M. Stengel, and G. Catalan, Physical review letters 115, 037601 (2015).